

Multi-Image Texture Analysis in Classification of Prostatic Tissues from MRI. Preliminary Results

Dorota Duda¹, Marek Kretowski¹, Romain Mathieu², Renaud de Crevoisier³,
and Johanne Bezy-Wendling³

¹ Faculty of Computer Science, Bialystok University of Technology, Poland
{d.duda,m.kretowski}@pb.edu.pl

² Department of Urology, Pontchaillou University Hospital, Rennes, France

³ LTSI, INSERM U1099, University of Rennes 1, France

Abstract. In the work, a (semi)automatic multi-image texture analysis is applied to the characterization of prostatic tissues from Magnetic Resonance Images (MRI). The method consists in a simultaneous analysis of several images, each acquired under different conditions, but representing the same part of the organ. First, the texture of each image is characterized independently of the others, using the same techniques. Afterwards, the feature values corresponding to the different acquisition conditions are combined in one vector, characterizing a multi-image texture. Thus, in the tissue classification process different tissue properties are considered simultaneously. We analyzed three MRI sequences: contrast-enhanced T1-, T2-, and diffusion-weighted one. Two classes of tissue were recognized: cancerous and healthy. Experiments with several sets of textural features and four classification methods showed that the application of multi-image texture analysis could improve the classification accuracy in comparison to single-image texture analysis.

Keywords: computer-aided diagnosis, tissue characterization, feature extraction, multi-image texture, classification.

1 Introduction

According to *Global Cancer Statistics* [1], prostate cancer is the second most frequently diagnosed cancer worldwide, and the sixth most frequent cause of cancer death in males. In 2008 it represented 14% of the total new cancer incidences (903,500 reported cases) and 6% of the total cancer deaths (258,400 cases) in males. In this context, the search for the methods allowing to detect a prostate pathology as early as possible and to determine its type (benign or malign) is crucial for reducing prostate cancer-caused mortality rates.

Admittedly, there exist some diagnostic tools for prostate cancers: the PSA (prostate-specific antigen) serum screening, the needle biopsies, or an ensemble of the MRI techniques enabling to visualize different prostatic tissue properties. However, the first two tools have many deficiencies and their use still remains

under discussion. For example, a 10-year experiment on 76,693 men conducted by Andriole *et al.* [2] revealed that there were no significant benefits of screening for prostate cancer with PSA serum testing. According to another report, in some cases prostate cancer screening could lead to over-treatment [3]. Furthermore, the use of needle biopsy, which is the current standard when discovering high PSA values, carries a risk of serious complications. Also, a needle may miss an important tumor case, when it does not hit the right place.

Considering the above facts, a large hope can be placed in a correct interpretation of MR prostate images, especially that their acquisition is not too invasive or harmful to health. However, the correct recognition of image content may go beyond the capacity of a non-equipped physician. It is important, therefore, to develop appropriate tools for computer-aided diagnosis (CAD).

The aim of present study is to validate methods for the texture-based analysis of MR prostate images and to examine their usefulness in prostatic tissue classification. In this process, we analyze simultaneously textures corresponding to different MR image sequences (contrast-enhanced T1-, T2-, and diffusion-weighted) and referring to the same prostate slice. According to our knowledge, no one has yet proposed a CAD system designed for prostate tumor recognition based on multi-image texture analysis from MR images. However, there exist few works on multi-image texture analysis concerning other organs and other imaging modalities. They have already shown that such an approach is promising in the process of tissue characterization and recognition.

The next section includes a short overview of existing CAD systems, incorporating methods for a simultaneous analysis of several images acquired under different conditions and representing the same part of an organ. In Sect. 3 our system for the classification of multi-image textures is presented. Experimental validation of the proposed methods is described in Sect. 4. Conclusions and future works follow in the last section.

2 Related Work

The earliest studies on the usefulness of multi-image texture analysis were presented in [4] and [5]. In both works, triples of CT liver images were analyzed simultaneously, in order to recognize the normal liver and its two primary malignant tumors: hepatocellular carcinoma (HCC) and cholangiocarcinoma. The images in a triple corresponded to the same liver slice. Each of them was acquired with different concentration of the contrast product injected to the patient. The first image was taken without the contrast, the next two ones – after its injection in the arterial and portal phase of its propagation in hepatic vessels. The multi-image texture was characterized by sets of features corresponding to each acquisition moment and placed all together in one vector. Experiments conducted separately for each of the three acquisition moments, and for the multi-image case proved the considerable potential of multi-image texture analysis.

The latter work, concerning the classification of liver pathologies from CT images, also showed the high usefulness of the multi-image approach for tissue characterization. In [6] four moments of contrast product propagation were considered: a pre-injection phase, and three after-injection phases: arterial, portal, and late. The CT images were analyzed in quadruples. Five types of liver lesions (cysts, adenomas, hemangiomas, HCC and metastasis) were recognized. Also here, a set of four textures was characterized by one vector composed of features calculated separately for each of the four acquisition moments.

Nagarajan *et al.* [7] used a multi-image texture analysis for breast lesion classification from dynamic contrast-enhanced (DCE) MR images. In order to differentiate two types of small lesions (benign and malignant) five post-contrast images were analyzed simultaneously. A multi-image texture was characterized by five values of the same textural feature, each corresponding to a different moment of contrast product propagation. The study showed that the characterization of the lesion enhancement pattern could improve the classification accuracy of the considered, diagnostically challenging, breast lesions.

Quite different approach to multi-image texture analysis was presented in [8]. This study introduces the notion of "textural kinetics" that characterizes texture evolution under contrast product propagation in DCE-MRI. At first, textural features are calculated at each moment of contrast product propagation, and the "textural kinetics curve" is created basing on the set of feature values. Afterwards, a third order polynomial is fitted to such curve in order to characterize its shape. Four polynomial coefficients constitute the feature vector. Such a method was applied to the recognition of benign and malignant breast lesions and proved to be superior to lesion intensity profile dynamics.

Finally, Bhooshan *et al.* [9] combined textural features from both DCE T1- and T2-weighted MR images in order to recognize benign and malignant breast lesions. For the T1-weighted sequences, only the first post-contrast image was used for texture analysis. In this case, contrast product propagation was characterized by typical kinetic parameters obtained from signal-to-time curves. The experiments showed, that the combination of texture characteristics, obtained from both T1-, and T2-weighted images may outperform the conventional analysis of T1-weighted contrast-enhanced sequences.

To the best of our knowledge, there is no such a CAD system that combines texture characteristics corresponding to different MRI sequences (like T1-, T2-, or diffusion-weighted) in order to characterize prostatic tissue in classification process. There exist a few systems that use information about the propagation of contrast product based on T1-weighted DCE-MR sequences (e.g. [10]). Nevertheless, they use only pharmacokinetic models, employing the signal-to-time curves in order to find perfusion parameters. The aim of our work is, therefore, to assess the utility of multi-image texture analysis in the characterization of prostatic tissue from MRI. The images belonging to different MRI sequences will be analyzed simultaneously.

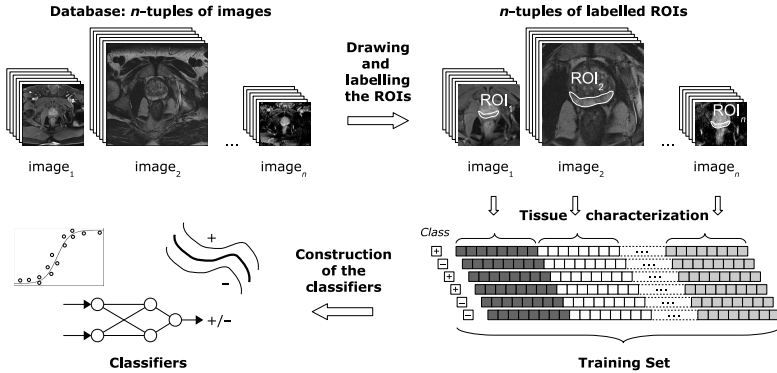


Fig. 1. A system for tissue classification based on multi-image texture analysis; the first stage of work: the construction of classifiers from a database of image n -tuples

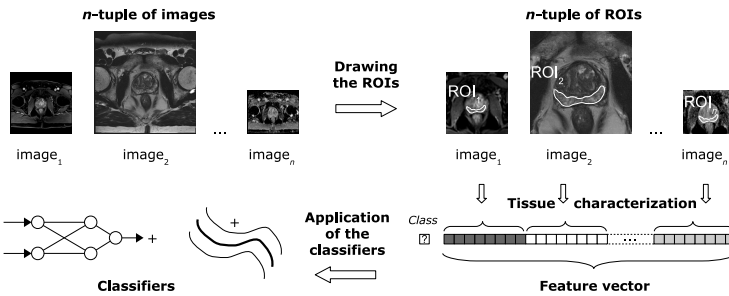


Fig. 2. A system for tissue classification based on multi-image texture analysis; the second stage of work: the application of classifiers to aid diagnosis

3 Methods

Two stages of work of a typical, image-based CAD system can be distinguished [11]. The first one, called *training* (or *learning*), consists in the preparation of the system for the recognition of several predefined tissue classes. In practice, this means constructing classifiers from a database of images which represent only diagnosed cases. The second stage is the application of the system in order to aid diagnosis.

The system which we are working on also follows the above-described, two-stage scheme. What distinguishes our system among others, is that the n images representing the same tissue slice but acquired under different acquisition conditions (e.g. different scanner settings) are combined in the n -tuples and analyzed simultaneously. The first stage of work of our system is presented in Fig. 1.

After the creation of a database, the n -tuples of images are formed. Depending on the number of considered image sequences, an n -tuple can comprise two, or more images. The order of images in each n -tuple is fixed. For example, a triple of

MRI prostate images might contain the T1-, the T2-, and the diffusion-weighted image on the first, the second, and the third position respectively.

An optional step here can be image pre-processing. It is used to improve the contrast, to eliminate the noise or the artifacts, or to equalize ranges of pixel values corresponding to different studies (which is the case in our database).

The next step is to outline the Regions of Interest (ROIs). A ROI covering the same part of the organ is outlined on each of the images forming an n -tuple. An n -tuple of thus obtained ROIs is analyzed simultaneously in order to characterize the tissue. First, the same set of textural features is calculated for each ROI in an n -tuple. Next, the features corresponding to different images in the n -tuple are combined in one "complex" vector characterizing a multi-image texture. In the simplest case, such a vector is formed by concatenating the sets of features corresponding to each considered sequence. Its parameters can also be a function of several feature values obtained with the same method and corresponding to different sequences. At this point, the doctor-specialist specifies the tissue class (label) which is attributed to each complex vector of features. The label reflects a pathology affecting the organ under consideration and is determined on the basis of a verified diagnosis. Labeled feature vectors form the so-called *training* (or *learning*) set. On the basis of such a set one or more classifiers are constructed.

Another optional step can be feature selection that takes place either before or during the construction of classifiers. It allows finding the most relevant features and rejecting redundant or inefficient ones. It also results in the reduction of memory and computation time required for the following processing steps.

Once the classifiers are constructed, the second stage of system work can take place: the system can be applied to identify new, yet undiagnosed cases. The key details of this process are depicted in Fig. 2.

At this stage, an n -tuple of images representing the same part of the organ is necessary. The order of the sequences from which subsequent images derive is the same as it was in the first stage of system work. Also the image pre-processing and the texture feature extraction techniques remain the same. After outlining the ROI on each of the images composing an n -tuple, the extraction of textural features for each ROI takes place. Next, a complex vector characterizing a n -tuple of textures is created. If feature selection was applied in the first stage, only the selected features are used here. Finally, the classifiers available in the system are applied and the most probable tissue class is indicated.

4 Experiments

The aim of the experiments was to assess the usefulness of the proposed method in the characterization of prostatic tissues from MR images. Three image sequences (contrast-enhanced T1-, T2-, and diffusion-weighted) were considered simultaneously in the classification of two tissue types: cancerous and healthy. Complex feature vectors were created by concatenating the parameters corresponding to the three sequences. For comparison, also pairs of image sequences were tested, as well as the one-sequence cases.

4.1 Database Description

The images were gathered in Pontchaillou University Hospital in Rennes, France, between August 2009 and April 2010. They were derived from 19 patients. One study per patient was available. The acquisitions were performed on a 3T Siemens *Verio* magnetic resonance scanner. The images were recorded in DICOM format. The T1-weighted sequences were taken after injection of a gadolinium-based contrast agent, *Dotarem*[®], in an amount of 13 to 20 ml. 30 different moments of contrast agent propagation were visualized. The time interval between consecutive moments was 7 seconds. The fat suppression (FS) method was applied for the T1 sequences. Slice thickness was the same for all the images of the same sequence: 3 mm for the T1-, and T2-weighted sequences, 6 mm for the diffusion-weighted ones. Image size in pixels was: 192×192 for the T1-weighted images, 320×320 (for 16 patients) or 448×448 (for 3 patients) for the T2-weighted ones, and 160×136 for diffusion-weighted. An example of the three corresponding images of considered sequences is given in the Figure 3.

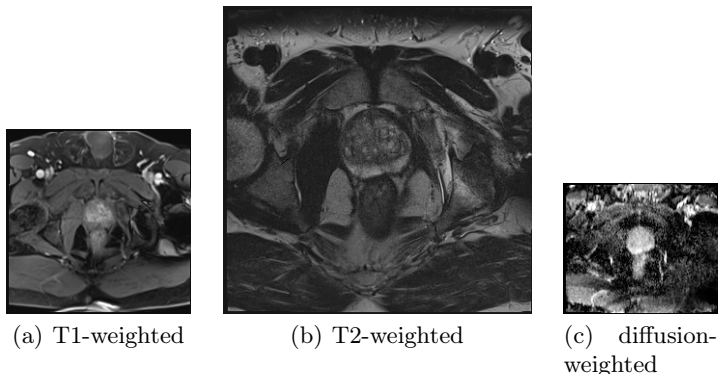


Fig. 3. Three MR images of prostate acquired at the same slice position; the proportions between images of each sequence were kept

In total, 180 ROIs were outlined for prostatic tissue, 60 for each of the three considered image sequences. Due to the fact that image sizes differed between sequences, the average sizes of ROIs corresponding to different sequences were also different. They amounted to 91, 456, and 85 pixels respectively.

For most studies, ROIs were outlined only within one of the two available classes (healthy or tumorous), which resulted in a certain inconvenience. It was not possible to determine the moment of contrast agent propagation in which the differences between texture characteristics corresponding to healthy and tumorous tissue were the most significant. For this reason, for our analyses, we always chose the middle image (15th of the available 30) from the T1-weighted sequences.

4.2 Image Conversion

An important drawback of our database was that the full range of pixel values possible to occur in the images (image resolution in pixel values) could not be determined from the DICOM headers. It is known that pixel values describing each organ fall into a certain part of the full range. Basing on pixel value histograms, obtained for the ROIs within the prostate, for the entire hips (not affected by tumor), and for the entire images, we hypothesized that image resolutions in pixel values might be different for each of the considered studies.

Therefore, in order to equalize the ranges of pixel values corresponding to different studies (separately for each sequence), the preliminary step of image processing was image conversion. Due to the fact that the ROIs outlined for the prostate were very small, and, for most studies, corresponded to only one tissue class, it would have been difficult to convert images basing only on the pixel values describing the prostate. Such a conversion was thus conducted in order to obtain the same range of pixel values (the smallest possible) corresponding to ROIs covering the hips.

In total, 1601 ROIs covering the hips were considered among which 678, 522, and 401 ROIs corresponded to T1-, T2-, and diffusion-weighted sequences respectively. Average ROI areas were about 547, 2404, and 412 pixels respectively. For each study and for each sequence, the range of pixel values was found separately. Each time, 5% of the brightest and the darkest pixels were not taken into account.

For the diffusion-weighted images the ranges of pixel values did not differ considerably. The widest of them were not even twice wider than the narrowest ones. The largest differences in ranges of pixel values were observed for T2 sequences. The widest range was more than nine times wider than the narrowest one. For T1 sequences it was above four times wider. The range centers obtained for different studies and the same series were located in different places.

Finally, the pixel values of the images of the T1-, and T2-weighted sequences were subjected to a linear transformation with integer coefficients. After the conversion, the range of gray levels sufficient to characterize all the pixels belonging to the prostate ROIs did not exceed 256, for each of the considered sequences. This allowed the images to be processed as if they were in a 8-bit BMP format.

4.3 Feature Extraction

The 30 texture features were calculated separately for each image in a triple. Six different approaches to texture analysis were used. They based on: autocorrelation (AC) [12], first order statistics (FO), gradients (GB), fractals (FB) [13], co-occurrence matrices (COM) [14], and run length matrices (RLM) [15, 16]. The names of features are given in Table 1.

For the COM and RLM methods, the number of gray levels was reduced to 64 and 32 respectively. The co-occurrence matrices were constructed separately for 4 standard directions (0° , 45° , 90° , and 135°), and for 2 different distances between the pixel pairs, 1 and 2. The run length matrices considered the 4 aforementioned

Table 1. Calculated textural features; the name of a feature set is created by adding the number of features (as a subscript index) to the name of the extraction method

Set	Feature Names
AC_2	$(d)Autocorr$, where $d = 1, 2$ is a pixel distance
FO_4	$Avg, Var, Skew, Kurt$
GB_4	$GradAvg, GradVar, GradSkew, GradKurt$
FB_1	$FractalDim$
COM_{11}	$AngSecMom, InvDiffMom, Entropy, Correlation, SumAvg, DiffAvg, SumVar, DiffVar, SumEntropy, DiffEntropy, Contrast$
RLM_8	$ShortEmp, LongEmp, GLNonUni, RLNonUni, Fraction, LowGLREmp, HighGLREmp, RLEntropy$

directions of pixel runs. Features obtained for different pixel distances and/or for different directions were averaged.

The normalized autocorrelation coefficients (AC method) were also calculated separately for 4 standard directions, and for 2 different pixel distances: 1, and 2. Only features corresponding to different directions were averaged.

The FB method was based on the fractional Brownian motion model [17] and also considered only 2 pixel distances, 1 and 2.

In total, 11 different feature sets were tested. Six of them contained features derived from one extraction method only. Another three sets combined features derived from several methods: All_{23} (COM, RLM, and FO), All_{25} (COM, RLM, FO, and AC), and All_{30} (all available features). Moreover, two sets of selected features were considered: Sel_F , and Sel_B . They contained features selected from the 30·3 possible ones (30 features corresponding to the 3 image sequences), using two searching directions, respectively *Forward*, and *Backward*. The selection of features was performed with the *Weka* software [18]. The following selection settings were applied: the wrapper method (called *WrapperSubsetEval* in *Weka*) – as an evaluator of each tested subset of features, the $C4.5$ tree [19] (*J48*) – as a classifier, and the *BestFirst* searching strategy.

4.4 Classification Results

Several classifiers were used in order to assess the potential of the multi-image texture analysis, and to compare it to that of one-sequence texture analysis. Among them were: logistic regression – LR (algorithm called *Logistic* in *Weka*), neural network – NN (*MultilayerPerceptron*), and support vector machines – SVM (algorithm *SMO*). The NN used a backpropagation algorithm and a sigmoid activation function. It had one hidden layer, wherein the number of neurons was equal to the average value of the number of features and the number of classes. The SVM used two kernels: the Gaussian kernel (*RBFKernel*), GK,

and the polynomial (*PolyKernel*) one, PK. The classification accuracies were estimated by 10-fold cross-validation, repeated 10 times.

The Table 2 presents selected results obtained for the classification of simple textures (when each sequence was considered separately) and multi-image textures (when three or two sequences were analyzed simultaneously). Each line of the table contains results obtained by the same classifier, for the same set of features, but for different image sequences (T1, T2 or diffusion) or image sequence combinations (T1 and T2, T1 and diffusion, T2 and diffusion, T1 and T2 and diffusion). We will always compare the results located in the same row of the Table 2 – obtained with the same classifier, and for the same set of features.

As for the cases of simple texture analysis, we can conclude that the most useful piece of information for the process of prostatic tissue classification was extracted from the T2- and the diffusion-weighted images. The advantage of the T2-weighted images was certainly that they were the biggest in size. Their drawback was the necessity of pre-conversion, as, initially, they showed the largest differences in the ranges of pixel values. Finally, taking into account the results obtained with T2-weighted images, we could estimate that the applied image conversion probably did not affect the classification results (too) negatively. Therefore, pre-conversion could be a good solution when no information about the full range of image pixel values is available in DICOM headers. In turn, inferior results obtained for a T1-weighted sequence may indicate the need to develop a method for choosing the most appropriate moment (in terms of tissue characterization) of contrast agent propagation.

The best classification results for the simple texture problem were: 94.83%, 95.67%, 93.00%, and 96.17% of correctly classified cases for the LR (with the Sel_F feature set), the NN (with COM_{11}), the SVM-GK (with Sel_F), and the SVM-PK (with All_{25}) classifiers respectively. Such results were obtained when the diffusion-weighted sequences (the case of the first three classifiers) or the T1-weighted sequences (the case of the last two classifiers) were considered.

Comparing classification results obtained for simple and multi-image textures, we can notice that there always exists at least one combination of two sequences that leads to better tissue recognition in comparison with the best possible one achieved for a single-sequence case. This is observed for each classifier, and for each feature set. The simultaneous analysis of images in triples almost always guaranties better results than the analysis of pairs of images. Finally, it is with the analysis of the three-image textures that the best overall classification result was achieved: 99.19%, for the combination of the SVM-PK classifier and the All_{23} feature set. With other classifiers the results slightly differed from the best possible one: 98.00%, 97.83%, and 98.00% obtained for the LR (with COM_{11}), NN (with RLM_8), and SVM-GK (with RLM_8 feature set) classifiers respectively.

The highest differences between the best results for the multi-image and the single-image case were observed with RLM_8 feature set: 7.00%, 6.33%, 6.50%, and 4.84% for the LR, the NN, the SVM-GK, and the SVM-PK classifiers respectively.

Table 2. Classification accuracy [%] (and standard deviation) obtained for simple and multi-image textures; three image sequences, T1-, T2-, and diffusion-weighted one ("Diff"), and four combinations of sequences were considered; the results were obtained using the four classifiers: logistic regression (LR), neural network (NN), support vector machines with a Gaussian kernel (SVM-GK) and with a polynomial kernel (SVM-PK)

Set of Features	Simple (One-Sequence) Textures				Multi-Image Textures			
	T1	T2	Diff	T1 and T2	T1 and Diff	T2 and Diff	T1 and T2 and Diff	
LR	<i>COM</i> ₁₁	68.67 (9.79)	87.33 (6.06)	93.50 (4.42)	96.17 (3.72)	91.17 (5.49)	92.83 (4.92)	98.00 (2.97)
	<i>RLM</i> ₈	75.17 (8.98)	90.00 (6.27)	85.00 (7.63)	91.17 (5.49)	87.33 (6.17)	89.33 (5.62)	97.00 (3.63)
	<i>Sel_F</i>	82.83 (7.54)	93.00 (5.32)	94.83 (4.39)	91.67 (5.23)	96.33 (4.03)	94.83 (4.39)	96.33 (4.03)
	<i>All</i> ₂₃	67.50 (9.87)	89.33 (5.87)	88.17 (6.41)	91.17 (5.62)	93.17 (5.31)	91.67 (5.49)	93.67 (5.14)
	<i>All</i> ₂₅	70.83 (9.28)	89.17 (6.09)	86.33 (7.05)	91.17 (5.98)	94.00 (4.82)	92.17 (5.36)	94.83 (4.84)
	<i>All</i> ₃₀	70.17 (8.73)	86.00 (6.13)	89.00 (6.29)	90.17 (5.82)	94.67 (4.57)	94.00 (5.37)	95.00 (4.67)
NN	<i>COM</i> ₁₁	78.17 (8.27)	90.67 (5.96)	95.67 (4.21)	96.83 (3.29)	95.33 (3.95)	95.83 (4.65)	96.50 (3.98)
	<i>RLM</i> ₈	77.50 (8.33)	91.50 (5.74)	90.17 (5.82)	97.83 (2.82)	87.83 (6.14)	92.00 (5.62)	97.33 (3.50)
	<i>Sel_F</i>	79.50 (7.19)	93.33 (5.43)	92.83 (4.92)	92.83 (5.33)	96.33 (4.03)	92.83 (4.92)	96.33 (4.03)
	<i>All</i> ₂₃	75.50 (7.99)	92.50 (5.35)	94.67 (4.87)	95.50 (3.72)	94.50 (4.28)	92.67 (4.93)	97.50 (3.43)
	<i>All</i> ₂₅	78.67 (8.79)	91.33 (5.36)	93.50 (5.29)	96.17 (3.90)	95.83 (4.00)	94.50 (4.89)	96.33 (3.86)
	<i>All</i> ₃₀	78.33 (8.91)	92.67 (4.93)	94.00 (4.02)	94.67 (4.42)	96.33 (3.67)	94.33 (4.77)	96.00 (4.29)
SVM-GK	<i>COM</i> ₁₁	67.67 (8.77)	92.17 (5.23)	88.67 (5.67)	88.83 (6.09)	93.00 (4.91)	93.67 (4.40)	94.83 (4.39)
	<i>RLM</i> ₈	73.00 (9.24)	91.50 (5.49)	89.67 (5.53)	94.33 (4.62)	91.17 (5.09)	96.67 (3.56)	98.00 (2.97)
	<i>Sel_F</i>	84.17 (6.85)	93.00 (4.91)	93.00 (4.62)	94.33 (4.77)	96.67 (3.75)	93.00 (4.62)	96.67 (3.75)
	<i>All</i> ₂₃	75.83 (8.90)	92.67 (4.79)	89.50 (5.51)	93.17 (4.75)	94.50 (4.89)	96.33 (3.47)	97.67 (2.91)
	<i>All</i> ₂₅	79.33 (7.87)	92.50 (4.80)	89.50 (5.39)	93.67 (5.40)	94.33 (4.77)	95.50 (3.90)	97.00 (3.43)
	<i>All</i> ₃₀	79.17 (7.98)	92.33 (5.22)	89.17 (5.61)	91.67 (5.74)	92.17 (5.23)	94.83 (4.69)	97.00 (3.43)
SVM-PK	<i>COM</i> ₁₁	77.00 (8.02)	96.00 (4.13)	93.33 (5.43)	96.83 (3.50)	96.17 (3.90)	96.50 (3.80)	98.00 (3.20)
	<i>RLM</i> ₈	79.50 (8.02)	93.33 (5.17)	91.00 (5.56)	97.00 (3.43)	93.00 (5.05)	95.50 (4.08)	98.17 (2.62)
	<i>Sel_F</i>	83.00 (7.11)	94.00 (4.52)	94.00 (4.52)	93.33 (4.89)	96.67 (3.75)	94.00 (4.52)	96.67 (3.75)
	<i>All</i> ₂₃	81.67 (7.06)	94.33 (4.62)	91.17 (5.62)	95.67 (3.86)	97.50 (3.43)	95.67 (4.37)	99.17 (2.48)
	<i>All</i> ₂₅	87.17 (6.79)	96.17 (4.08)	91.33 (5.36)	96.33 (3.86)	98.00 (2.97)	96.00 (4.29)	98.67 (2.56)
	<i>All</i> ₃₀	81.67 (7.72)	93.67 (5.14)	95.17 (4.63)	96.33 (3.86)	97.00 (3.63)	96.17 (3.90)	98.33 (2.78)

5 Conclusions and Future Work

In the work, a multi-image texture analysis was applied, for the first time, to the characterization of prostatic tissues from MR images. Images representing the same prostate slice but corresponding to different acquisition conditions (giving the T1-, T2-, and diffusion-weighted sequences) were analyzed simultaneously. Two classes of prostatic tissue were recognized: cancerous and healthy.

Experiments have shown that a simultaneous analysis of two, or three images can improve the recognition of prostatic tissues, in comparison with single-image analysis. The best results obtained for multi-image (two-, or three-image) cases were better than the best corresponding ones achieved for simple-image cases. The best improvement of classification quality reached 7.00%. The analysis of three-image textures proved to ensure the best classification result.

We admit that the preliminary experimental results, although promising, could also be subject to error. This could have been avoided if a key piece of information had been available in the database to process, namely the full ranges of image pixel values, apparently different for different studies. In this case, image conversion based on the analysis of the intervals of pixel values corresponding to another organ (in our case the hips) seemed to be the only solution. Nevertheless, the texture of the hips can also be altered by the presence of various pathological processes, different for each patient. To avoid this problem in the future, either image acquisition protocols should be standardized or images should contain information about the full ranges of pixel values. Furthermore, when acquiring images, a good idea would be to place a "reference object" in view. The texture analysis of such an object could be crucial for the purposes of image conversion aimed at the equalization of pixel value ranges corresponding to different studies.

Finally, it would be desirable to have two types of ROIs (corresponding to cancerous and healthy tissue) delineated for each study or patient. Such an information would allow to analyze changes in texture characteristics under contrast product propagation (in T1-weighted sequences) corresponding to the both types of tissue. Basing on such an analysis one could determine which moment of contrast product propagation is related to the most significant differences in texture characteristics obtained for cancerous and healthy tissue.

In the future, we will try to resolve all of the aforementioned problems. It would be worthwhile to repeat the experiments using a much larger database and to recognize more than two tissue classes. Other MRI sequences, such as FLAIR (fluid-attenuated inversion recovery) or proton density-weighted, can also be considered for multi-image texture analysis. It also seems to be interesting to find a method for characterizing texture evolution under contrast product propagation based on the simultaneous analysis of many contrast-enhanced T1-weighted images related to different concentrations of the contrast product in prostatic vessels.

Acknowledgement. This work was supported by the grant S/WI/2/2013 from Bialystok University of Technology.

References

1. Jemal, A., Bray, F., Center, M.M., et al.: Global cancer statistics. *CA: A Cancer J. Clin.* 61(2), 69–90 (2011)
2. Andriole, G.L., Crawford, E.D., Grubb, I.R.L., et al.: Mortality Results from a Randomized Prostate-Cancer Screening Trial. *N. Engl. J. Med.* 360, 1310–1319 (2009)
3. Greene, K.L., Albertsen, P.C., Babaian, R.J., et al.: Prostate Specific Antigen Best Practice Statement: 2009 Update. *J. Urol.* 182(5), 2232–2241 (2009)
4. Duda, D., Krętowski, M., Bézy-Wendling, J.: Texture-based classification of hepatic primary tumors in multiphase CT. In: Barillot, C., Haynor, D.R., Hellier, P. (eds.) MICCAI 2004. LNCS, vol. 3217, pp. 1050–1051. Springer, Heidelberg (2004)
5. Duda, D., Kretowski, M., Bezy-Wendling, J.: Texture characterization for Hepatic Tumor Recognition in Multiphase CT. *Biocybern. Biomed. Eng.* 26(4), 15–24 (2006)
6. Quatrehomme, A., Millet, I., Hoa, D., Subsol, G., Puech, W.: Assessing the classification of liver focal lesions by using multi-phase Computer Tomography scans. In: Greenspan, H., Müller, H., Syeda-Mahmood, T. (eds.) MCBR-CDS 2012. LNCS, vol. 7723, pp. 80–91. Springer, Heidelberg (2013)
7. Nagarajan, M.B., Huber, M.B., Schlossbauer, T., Leinsinger, G., Krol, A., Wismüller, A.: Classifying small lesions on breast MRI through dynamic enhancement pattern characterization. In: Suzuki, K., Wang, F., Shen, D., Yan, P. (eds.) MLMI 2011. LNCS, vol. 7009, pp. 352–359. Springer, Heidelberg (2011)
8. Agner, S.C., Soman, S., Libfeld, E., et al.: Novel kinetic texture features for breast lesion classification on dynamic contrast enhanced (DCE) MRI. In: Proc. of SPIE, vol. 6915(69152C) (2008)
9. Bhooshan, N., Giger, M., Lan, L., et al.: Combined use of T2-weighted MRI and T1-weighted dynamic contrast-enhanced MRI in the automated analysis of breast lesions. *Magn. Reson. Med.* 66(2), 555–564 (2011)
10. Sung, Y.S., Kwon, H.J., Park, B.W., et al.: Prostate cancer detection on dynamic contrast-enhanced MRI: computer-aided diagnosis versus single perfusion parameter maps. *Am. J. Roentgenol.* 197(5), 1122–1129 (2011)
11. Duda, D.: Medical image classification based on texture analysis. PhD Thesis, University of Rennes 1, Rennes, France (2009)
12. Gonzalez, R.C., Woods, R.E.: *Digital Image Processing*, 2nd edn. Addison-Wesley, Reading (2002)
13. Chen, C., Daponte, J.S., Fox, M.D.: Fractal feature analysis and classification in medical imaging. *IEEE Trans. Med. Imag.* 8(2), 133–142 (1989)
14. Haralick, R.M., Shanmugam, K., Dinstein, I.: Textural features for image classification. *IEEE Trans. Syst. Man Cybern.* 3(6), 610–621 (1973)
15. Galloway, M.M.: Texture analysis using gray level run lengths. *Comp. Graph. and Im. Proc.* 4(2), 172–179 (1975)
16. Chu, A., Sehgal, C.M., Greenleaf, J.F.: Use of gray value distribution of run lengths for texture analysis. *Pattern Recog. Lett.* 11(6), 415–419 (1990)
17. Chen, E.L., Chung, P.C., Chen, C.L., et al.: An automatic diagnostic system for CT liver image classification. *IEEE Trans. Biomed. Eng.* 45(6), 783–794 (1998)
18. Hall, M., Frank, E., Holmes, G., et al.: The WEKA data mining software: an update. *SIGKDD Explorations* 11(1), 10–18 (2009)
19. Quinlan, J.: *C4.5: Programs for Machine Learning*. Morgan Kaufmann, San Francisco (1993)